Quarterly Reviews of Biophysics **37**, 1 (2004), pp. 3–13. © 2004 Cambridge University Press
DOI: 10.1017/S0033583504003920 Printed in the United Kingdom

ESSAY

Realizing the potential of electron cryo-microscopy

Richard Henderson

MRC Laboratory of Molecular Biology, Hills Road, Cambridge CB2 2QH, UK

Abstract. Structural analysis by electron microscopy of biological macromolecules or macromolecular assemblies embedded in rapidly frozen, vitreous ice has made great advances during the last few years. Electron cryo-microscopy, or cryo-EM, can now be used to analyse the structures of molecules arranged in the form of two-dimensional crystals, helical arrays or as single particles with or without symmetry. Although it has been possible, using crystalline or helical specimens, to reach a resolution adequate to build atomic models (4 Å), there is every hope this will soon also be possible with single particles. Small and large single particles present different obstacles to progress.

1. Introduction

In 1984, Dubochet and colleagues published a stunning picture of adenovirus (Fig. 1), beautifully preserved in rapidly frozen amorphous ice. This pioneering development in specimen preparation opened up the possibility that biological structures could be determined by electron microscopy (EM) of frozen unstained specimens at a variety of levels of detail. Although others had studied frozen specimens by EM earlier (Taylor & Glaeser, 1976; Heide, 1982), they had either found the cryo-transfer difficult or had not been able to reach sufficiently low temperatures for the ice to remain non-crystalline. The work of Dubochet and colleagues can thus properly be termed the birth rather than conception of electron cryo-microscopy (cryo-EM). This

Tel.: +44-1223-402215; Fax: +44-1223-249565; E-mail: rh15@mrc-lmb.cam.ac.uk

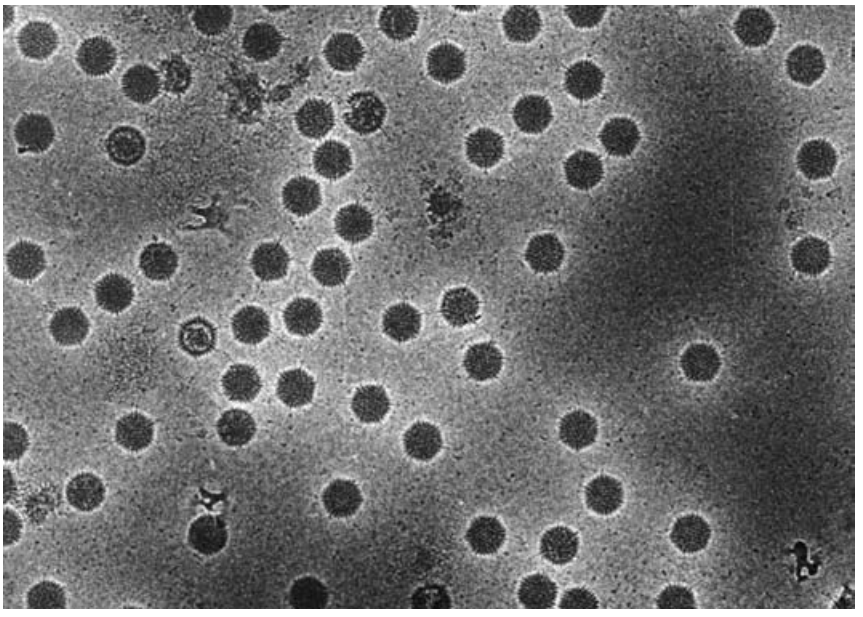

Fig. 1. Electron micrograph of adenovirus virions, with occasional damaged particles, embedded in rapidly frozen vitreous ice. This picture was taken over 20 years ago by Adrian *et al.* (1984) and appeared on the cover of the issue of *Nature* in which their pioneering article was published. Micrographs like these were later analysed to produce valuable insights into the structure of adenovirus (Stewart *et al.* 1991, 1993).

approach opened up the possibility of three-dimensional (3D) atomic structures through precise, very high-resolution microscopy of homogeneous particulate molecular assemblies, which lie in random orientations on the grid. For larger non-particulate specimens, cellular tomography by combination of micrographs of tilt series from thin layers of frozen cells or subcellular components provided an alternative approach. Outstanding progress has been made in both these areas, providing a wealth of information not obtainable by any other methods.

During the last 10 years or so, a number of atomic structures, predominantly of membrane proteins, have been determined by cryo-EM of two-dimensional (2D) crystals. In addition, during the last year, cryo-EM of two helical assemblies, those of tubular arrays of *Torpedo* acetylcholine receptors and of the bacterial flagellum, has produced maps at sufficient resolution (4 Å) to build excellent atomic models showing most of the atoms in each structure. EM of 2D crystals and helical one-dimensional (1D) crystals both make use of the precise internal geometrical relationship between identical, repeating molecular structures to improve the signal-to-noise ratio by averaging of intrinsically noisy images, which are limited by the electron statistics.

By contrast, the extended geometrical arrangement in 1D or 2D crystals is absent in micrographs of single particles, although the particles may have internal symmetry. The relative position and orientation of each particle must be determined before the information from all the particles can be averaged together. Similarly, tomographic reconstructions require the combination of a large number of views of an individual field taken from many different angles to allow the calculation of a 3D map of a biological structure or cellular volume. Nevertheless, the technique, the philosophy and the equipment required to span these different approaches to biological structure determination are sufficiently similar to be discussed together here under

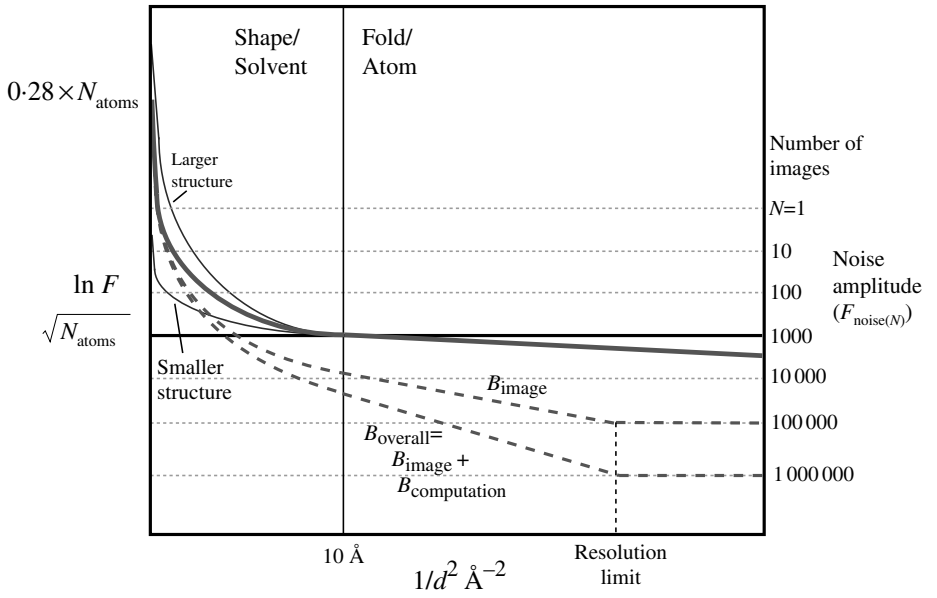

Fig. 2. Schematic diagram showing the typical variation of the logarithm of the average scattering amplitude ($\ln F$) from a macromolecule as a function of $1/d^2$, where d is the resolution (Å). The amplitude at the origin on the left is proportional to N_{atoms}, the total number of atoms in the molecular mass (in carbon atom equivalents) multiplied by the solvent contrast (0·28) and this places the scattering on an absolute scale. The protein scattering curve (thick continuous line) consists of a low-resolution region ($d > 10$ Å) determined by molecular shape and solvent contrast, and a high-resolution region ($d < 10$ Å) which approaches the scattering of randomly placed atoms described by Wilson statistics. This decreases only slightly with resolution and can be approximated by the horizontal line of amplitude $\sqrt{N_{atoms}}$. The high-resolution region may also have structure corresponding to fold-specific features, including α-helix and β-sheet, but this possible variation is not shown in the diagram. The average noise amplitude is $F_{noise(1)}$ for a single image or $[F_{noise(1)}/\sqrt{N}]$ after averaging N images and examples are shown for values of N between 1 and 1 000 000 (dashed and regularly spaced horizontal lines). Low-resolution structure factor amplitudes are also shown for a large structure such as might be studied by tomography and for a small molecular mass particle which has a low-resolution scattering amplitude below the noise level for one image (thin continuous lines). The experimental contrast loss for structure factors at high resolution due to imperfect images is indicated by a dashed line labelled by its slope, the temperature factor B_{image}. Additional contrast lost due to imperfect computations, such as error in orientation determination, gives a line with slope $B_{overall}$, which is the sum of temperature factors B_{image} and $B_{computation}$. The resolution limit for any experimental data-set occurs where the structure factor curve falls to the point where it equals the noise level. In this example, the desired resolution limit is shown at 6·4 Å and is found for 10^6 particles for $B_{overall}$, but at 10^5 particles if $B_{computation} = 0$. [A more detailed explanation about this can be found in Rosenthal & Henderson (2003) from which the diagram has been reproduced, with permission.]

the heading of 'electron cryo-microscopy'. This brief essay aims to provide a snapshot of the progress and prospects in the field in early 2004.

2. Background

A useful overview of the fundamental limiting constraint in cryo-EM is shown in Fig. 2, taken from Rosenthal & Henderson (2003), which is based on some entirely theoretical calculations published nearly 10 years ago (Henderson, 1995). The key factor governing the

information present in any electron micrograph of unstained biological material is radiation damage. It is an unfortunate fact that the desirable elastic scattering of electrons by the atoms making up a structure is accompanied by inelastic interactions which deposit energy in the specimen and, in the case of organic and biological specimens, result in the destruction of the delicate covalent bonding which holds together the structure. Each inelastic scattering event, of which there are 3–4 for every elastic scattering event, deposits an energy of ~ 20 eV on average which is more than enough to ionize parts of the structure, break covalent bonds and create free radicals. As a result the debris of the exposure of a biological specimen to a typical electron dose consists of hundreds of different products which resemble the chemically homogeneous starting sample to a greater or lesser extent. These radiolytic products, which are very similar whether the incident radiation comes from electrons, X-rays or neutrons, include some small, mobile fragments as well as a few with additional cross-links. The smaller fragments can be restrained from moving from their initial location by cooling the specimen to low temperatures. The smallest radiolytic fragments require the lowest temperatures to become immobilized. Hence, it is accepted that keeping the specimen at the lowest temperature possible can, in principle, ensure that the structure of the radiation-damaged specimen will retain its similarity to the unirradiated starting sample to the greatest degree. In practice, the choice is between specimens cooled to near liquid nitrogen or those cooled to near liquid helium temperatures. Use of liquid helium-cooled specimens requires greater care due to the decreased conductivity of carbon support films which can cause greater charging, and the lower latent heat for the evaporation of helium which can cause boiling, vibration of the specimen support stage and lower resolution in the image. However, provided the practical problems are solved, the use of a microscope capable of cooling the specimen to liquid helium temperature should give more information from each micrograph.

A key requirement for specimens embedded in vitreous ice, first shown by Dubochet and colleagues (Adrian *et al.* 1984; Dubochet *et al.* 1988), is that the specimen must be kept below a temperature of appproximately $-150\ ^{\circ}$C to prevent formation of either cubic or hexagonal ice and to ensure that the amorphous structure of the supporting aqueous solution is retained. Depending on the required resolution in the structure determination, electron exposures between 5 and 25 e/Å^2 are normally possible. However, the 'safe' dose for very high-resolution work, by extrapolation from recent X-ray damage studies of crystals of bacteriorhodopsin where the chromophore begins to be affected at 2×10^{14} photons/mm^2 (Matsui *et al.* 2002), is very low indeed at $\sim 0{\cdot}1$ e/Å^2, so we need to be alert to possible radiation damage effects even at very low doses. After an exposure of, for example, 10 e/Å^2, a second exposure taking the accumulated dose to 20 e/Å^2 will still provide an image of the specimen which resembles the first image, but it will have much lower resolution due to the changed structure of the specimen following irradiation.

The noise level in a structure determined from one such exposure, or from a series of exposures in which the total dose is equivalent to ~ 5 e/Å^2, is shown by the line labelled $N=1$ in Fig. 2. As more images are added the amplitude of the noise in any map, relative to the signal, drops proportionally to $\sqrt{N}$ and this is shown by the horizontal dashed lines at lower amplitude in Fig. 2. The criterion for whether the structure can be observed above the noise level thus depends on the average amplitude of the structure being observed (thick curved continuous or dashed lines) relative to the noise level. At low resolution, large molecular assemblies with larger amplitudes are therefore easier to observe, but at high resolution, remarkably, beyond a Fourier

Table 1. *2D and 1D structures beyond 10 Å resolution*

Structure	Resolution	Reference
Two-dimensional crystals [high resolution (better than 4 Å)]		
Bacteriorhodopsin p3	3·5 Å, 3·0 Å	Henderson *et al.* (1990), Kimura *et al.* (1997)
Plant LHC-II	3·4 Å	Kühlbrandt *et al.* (1994)
Tubulin dimmer	3·7 Å	Nogales *et al.* (1998)
Aquaporin	3·8 Å, 4·0 Å	Murata *et al.* (2000), Mitra *et al.* (2002)
Two-dimensional crystals [low resolution (better than 9 Å)]		
Bacteriorhodopsin orthorhombic	6·5 Å	Leifer & Henderson (1983)
Deoxycholate bacteriorhodopsin	6·0 Å	Tsygannik & Baldwin (1987)
Halorhodopsin	5·0 Å	Kunji *et al.* (2000)
Porin PhoE	6·0 Å	Jap *et al.* (1991)
Plant photosystem II RC	8·0 Å	Rhee *et al.* (1998)
Yeast H^+-ATPase	8·0 Å	Auer *et al.* (1998)
Gap junction channel	7·5 Å	Unger *et al.* (1999)
Glutathione transferase	6·0 Å	Schmidt-Krey *et al.* (2000)
NhaA Na/H antiporter	7·0 Å	Williams (2000)
Glycerol channel GlpF	6·9 Å	Stahlberg *et al.* (2000)
Rhodopsin, frog p2	7·5 Å	Unger *et al.* (1997)
Rhodopsin, bovine $p22_12_1$	5·5 Å	Krebs *et al.* (2003)
OxlT, oxalic acid transporter	6·5 Å	Hirai *et al.* (2002)
SecYEG complex	8·0 Å	Breyton *et al.* (2002)
EmrE multidrug transporter	7·0 Å	Ubarretxena-Belandia *et al.* (2003)
Helical structures		
Acetylcholine receptor	4·0 Å	Miyazawa *et al.* (2003)
Bacterial flagellum	4·0 Å	Yonekura *et al.* (2003)
Microtubule	8·0 Å	Li *et al.* (2002)
Calcium ATPase	8·0 Å	Zhang *et al.* (1998)
Tobacco mosaic virus	10·0 Å	Jeng *et al.* (1989)

spacing of $\sim\frac{1}{10}$ Å^{-1}, where Wilson statistics give a good estimate of the average structure factor, the number of images needed to reach a given signal-to-noise ratio is almost independent of the size of the structure being observed (Henderson, 1995).

3. 2D crystals

There are now four molecular structures for which atomic models were determined by EM of 2D crystals at resolutions of 4 Å or better (Table 1, first section). The methods used were first worked out on bacteriorhodopsin (Henderson *et al.* 1990). In addition, many other structures have been determined at lower resolutions (in the range 5–8 Å), which have nevertheless allowed the structural arrangement of α-helices to be defined (Table 1, second section). This is particularly useful for membrane proteins where the existence of other constraints and observations about the structure can often allow the complete topography to be determined, including the identification of which α-helices correspond to which parts of the amino-acid sequence [e.g. OxlT (Hirai *et al.* 2003), bacteriorhodopsin (Engelman *et al.* 1980) and rhodopsin (Baldwin *et al.* 1997)]. Experience has shown that a resolution of better than 4 Å is

needed before it is possible to recognize features well enough to make a unique assignment of side-chains to a sequence of amino acids, with bulky side-chains being most easily recognized.

4. 1D crystals (helical arrays)

In this group, listed in the final section of Table 1, there are now two membrane proteins and three structures which naturally form filamentous assemblies. The structure determinations of naturally occurring microtubules and bacterial flagella have resulted in structures at 8 and 4 Å resolution respectively, whereas the older work on tobacco mosaic virus was at 10 Å resolution. In the case of microtubules, this has allowed interpretation of the density in terms of a complete atomic model of the microtubule since the atomic model of the $\alpha\beta$-tubulin dimer obtained from electron 2D crystallography could be positioned and oriented in the density from the helical structure determination. Similarly, the interpretation of the structure of the bacterial flagellum was helped by the X-ray structure of a proteolytic fragment of flagellin, the protein subunit (Samatey *et al.* 2001).

Of the two membrane proteins, the structure analysis of the nicotinic acetylcholine receptor tubes has reached the highest resolution (4 Å) and this has allowed interpretation of the density in terms of an atomic model. The interpretation of the structure of the extracellular acetylcholine-binding domain was helped by the availability of an X-ray structure of the pentameric acetylcholine-binding protein from the synapse of a mollusc (Brejc *et al.* 2001). The membrane part of each of the five subunits is made up of four transmembrane α-helices which have a characteristic shape. The existence of a pseudo-fivefold symmetry within the resulting bundle of 20 transmembrane helices also helped interpretation in terms of the amino-acid sequence. The tubes of Ca^{2+}–ATPase were taken to 8 Å (Zhang *et al.* 1998) before an X-ray atomic structure was determined (Toyoshima *et al.* 2000).

The critical resolution of 4 Å which allows density to be recognized and interpreted in terms of an atomic model has thus been reached for two different helical structures. The two 8 Å resolution structures can be understood by reference to the atomic models of the same protein in an X-ray or 2D crystal structure. The microtubule structure, after docking of the $\alpha\beta$-tubulin model, provided key information about contact residues between protofilaments. The comparison of X-ray and EM domain arrangements, for Ca^{2+}–ATPase in different functional states, helped to define the likely structural changes during calcium pumping.

5. Icosahedral single particles

Naturally occurring icosahedral assemblies with 532 point group symmetry consist mostly of virus structures, some having 60 identical subunits, some having a greater number of subunits with additional quasi-symmetry, such as virions with 180 ($T=3$) or 240 ($T=4$) chemically identical subunits and some built from molecules of more than one kind. Because these icosahedral particles tend to be much larger than particles with lower symmetry, giving rise to images containing more information per particle, it is technically easier to determine the particle orientations, so that the achievable resolution is limited more by the intrinsic quality of the specimen or the cryo-EM rather than any limitations of the computer programs or the signal-to-noise ratio in the particle images. As a result, there are now more than 10 structures of

Table 2. *Single particle structures beyond 10 Å resolution*

Structure	MW[a]	Resolution	Reference
Icosahedral structures			
Hepatitis B cores	4·1 MDa	7·4 Å, 9 Å	Böttcher *et al.* (1997), Conway *et al.* (1997)
Herpes virus capsid	192 MDa	8·5 Å	Zhou *et al.* (2000)
Cytoplasmic polyhedrosis virus	>40 MDa	8 Å	Zhou *et al.* (2003)
Semliki Forest virus	48 MDa	9 Å[b]	Mancini *et al.* (2000)
PM2 virus	47 MDa	8·5 Å	Huiskonen *et al.* (In Press)
Sindbis virus	46 MDa	∼11 Å	Zhang *et al.* (2002)
Dengue virus	>13 MDa	9·5 Å	Zhang *et al.* (2003a)
Reovirus virions	110 MDa	7·6 Å	Zhang *et al.* (2003b)
Pyruvate dehydrogenase, E2CD	1·5 MDa	8·7 Å	Rosenthal & Henderson (2003)
Rice dwarf virus	53 MDa	6·8 Å	Zhou *et al.* (2001)
Tomato bushy stunt virus	8·9 MDa	5·9 Å[c]	van Heel *et al.* (2000)
P22 bacteriophage mature/shell	50/20 MDa	9·5/8·5 Å	Jiang *et al.* (2003)
Single particles of lower[d] symmetry than icosahedral			
E. coli 70S ribosome	2·5 MDa	11·5 Å, 9 Å	Gabashvili *et al.* (2000), Valle *et al.* (2003)
Bacteriophage SPP1 connectors	1·0 MDa	10 Å	Orlova *et al.* (2003)
50S ribosomal subunit	1·6 MDa	7·5 Å[e]	Matadeen *et al.* (1999)
GroEL	0·8 MDa	8·7 Å, 11·5 Å	Ranson *et al.* (2001), Ludtke *et al.* (2001)

[a] The molecular weights (MW), for the virus particles in the table, refer to the icosahedrally ordered parts of the structures, which are, in most cases, the protein components.

[b] Note that, in this case, the map was calculated to 9 Å resolution, but a more conservative criterion indicates a resolution of 10·4 Å at best.

[c] In this case, the resolution is based on a 3σ noise criterion which is not comparable to the other entries. The equivalent resolution using the criterion recently proposed (Rosenthal *et al.* 2003) is ∼8 Å.

[d] Note that single particles with lower symmetry usually have a smaller size than icosahedral particles with 60-fold symmetry. However, it is the smaller size rather than the lower symmetry which makes these smaller structures more challenging to determine.

[e] Note that this resolution is based on a 3σ noise criterion which is not comparable to the other entries. A comparable figure to the others is likely to be ∼10 Å.

icosahedral particles which have reached resolutions better than ∼10 Å, and these are listed in Table 2 (first section). In future, with inclusion of greater numbers of particles, it should be possible to reach even higher resolution and in favourable cases cross the 4 Å barrier where the density can be directly interpreted in terms of the amino-acid sequence and used to derive an atomic model.

In the case of the two highest resolution structures obtained so far, those of hepatitis B cores (Böttcher *et al.* 1997) and rice dwarf virus (Zhou *et al.* 2001), the proposed polypeptide chain folds based on the cryo-EM maps were subsequently found to be correct by X-ray crystallographic analyses at near-atomic resolution (Wynne *et al.* 1999; Nakagawa *et al.* 2003).

6. Single particles with lower symmetry

The biggest challenge for the future for cryo-EM lies in this area. Most biological structures do not naturally form icosahedral (I) assemblies, nor 1D or 2D crystals. As a result, the molecular weight of particles with either no symmetry or with cyclic (Cn), dihedral (Dn), tetrahedral (T) or

octahedral (O) symmetry is relatively low and this means the information content of the electron microscope images of each particle is limited. It follows that the accuracy of the determination of the position and orientation of the particles is also limited with a resulting reduction in the resolution of the final map. In addition, it is possible that beam-induced movement or changes in orientation during the electron exposure may be greater for these smaller particles than for larger icosahedral particles or for helical or crystalline arrays. As can be seen in Table 2 (second section), the best resolutions achieved for these smaller macromolecular assemblies have only just reached 10 Å. The challenge for the future is therefore to identify the limiting factors and make improvements in experimental protocols and computational procedures to allow these present limitations to be overcome. Alongside improved images, it is likely that, for larger particles, a more precise correction of spatial image distortions will be needed alongside correction for curvature of the Ewald sphere (DeRosier, 2000), whereas for smaller particles a more reliable orientation parameter determination will be required.

7. Cellular and subcellular electron tomography

The recent paper by Medalia *et al.* (2002) has clearly demonstrated that cellular ultrastructure including membranes, microtubules and microfilaments with associated macromolecular assemblies (ribosomes, proteosomes, etc.) can be revealed using electron cryo-tomography. Other laboratories (see Horowitz *et al.* 1994; Bullit *et al.* 1997; O'Toole *et al.* 1999; Chen *et al.* 2001) have published electron tomographic analyses using similar methods but at lower resolutions. Figure 2 also shows, from a theoretical viewpoint, that electron tomography of thin frozen specimens should be able to reach resolutions of $\sim$20 Å but not beyond. In this case, the allowed total electron dose, which might be used to produce a single projected image for a field of identical particles (noise level $N=1$ in Fig. 2), must be distributed over the whole tilt series. Ultimately, radiation damage thus places an absolute limit on the resolution of EM structure determination without the benefit of averaging. This limit can be extended when images of identical macromolecular assemblies are averaged to produce higher resolution 3D maps. Nevertheless, there is great potential for the use of electron tomography in cell biology.

8. Conclusion and future prospects

Given the good progress already made, it is entirely reasonable to expect the consolidation and simplification of biological structure determination by cryo-EM using 2D or helical arrays, resulting in a growing number of very valuable structure determinations that sometimes cannot be obtained by any other approach. Similarly, the analysis of unique structures such as those found in living cells or subcellular organelles by electron tomography should become simpler and quicker whilst being limited to resolutions of $\sim\frac{1}{20}$ Å^{-1}.

However, it is in the area of single particle cryo-EM that I expect to see most progress. Structural analysis of symmetrical and asymmetrical structures should increase in power with technical and computational improvements so that structures at improved resolutions are obtained. I hope that within the next few years we will see 4 Å resolution structures from single-particle EM giving maps with resolution adequate to assign a sequence of amino-acid side-chains into particular density features. Alongside these 'high-resolution' structure determinations, there should be many other studies at lower resolutions which will provide answers to burning

questions when juxtaposed with the knowledge of the atomic structures of individual domains from other techniques such as X-ray crystallography or nuclear magnetic resonance spectroscopy. Finally, methods used to analyse the structures of mixed or dynamic populations, where a particular macromolecular assembly cannot be trapped in a homogeneous state but where images of the structure can be classified into groups, will continue to be developed and will have increasing value.

Alongside these trends, I also hope that rigorous validation methods and criteria will be developed which can prove whether a given structure determination is reliable. This is particularly important when low-resolution structures are being determined. For resolutions better than 4 Å, the agreement of the density with the known amino-acid sequence acts as an independent internal control but, at lower resolution, the current cyclical refinement procedures produce a self-consistent result which lacks rigorous proof of correctness. Procedures such as the one developed by Rosenthal & Henderson (2003), where pairs of images of a field of particles with different tilt are used to analyse the accuracy of orientation parameter determination, may help. Nevertheless, development of a wider range of validation tools is probably the biggest challenge facing cryo-EM.

9. References

Adrian, M., Dubochet, J., Lepault, J. & McDowall, A. W. (1984). Cryo-electron microscopy of viruses. *Nature* **308**, 32–36.

Auer, M., Scarborough, G. A. & Kühlbrandt, W. (1998). Three-dimensional map of the plasma membrane H^+-ATPase in the open conformation. *Nature* **392**, 840–843.

Baldwin, J. M., Schertler, G. F. X. & Unger, V. M. (1997). An alpha-carbon template for the transmembrane helices in the rhodopsin family of G-protein-coupled receptors. *Journal of Molecular Biology* **272**, 144–164.

Böttcher, B., Wynne, S. A. & Crowther, R. A. (1997). Determination of the fold of the core protein of hepatitis B virus by electron cryo-microscopy. *Nature* **386**, 88–91.

Brejc, K., van Dijk, W. J., Klaassen, R. V., Schuurmans, M., van der Oost, J., Smit, A. B. & Sixma, T. K. (2001). Crystal structure of an ACh-binding protein reveals the ligand-binding domain of nicotinic receptors. *Nature* **411**, 269–276.

Breyton, C., Haase, W., Rapoport, T. A., Kuhlbrandt, W. & Collinson, I. (2002). Three-dimensional structure of the bacterial protein-translocation complex SecYEG. *Nature* **418**, 662–665.

Bullit, E., Rout, M. P., Kilmartin, J. V. & Akey, C. W. (1997). The yeast spindle pole body is assembled around a central crystal of Spc42p. *Cell* **89**, 1077–1086.

Chen, L. F., Blanc, E., Chapman, M. S. & Taylor, K. A. (2001). Real space refinement of acto-myosin structures from sectioned muscle. *Journal of Structural Biology* **133**, 221–232.

Conway, J. F., Cheng, N., Zlotnick, A., Wingfield, P. T., Stahl, S. J. & Steven, A. C. (1997). Visualization of a 4-helix bundle in the hepatitis B virus capsid by cryo-electron microscopy. *Nature* **386**, 91–94.

DeRosier, D. J. (2000). Correction of high-resolution data for curvature of the Ewald sphere. *Ultramicroscopy* **81**, 83–98.

Dubochet, J., Adrian, M., Chang, J. J., Homo, J. C., Lepault, J., McDowall, A. W. & Schultz, P. (1988). Cryo-electron microscopy of vitrified specimens. *Quarterly Reviews of Biophysics* **21**, 129–228.

Engelman, D. M., Henderson, R., McLachlan, A. D. & Wallace, B. A. (1980). Path of the polypeptide in bacteriorhodopsin. *Proceedings of the National Academy of Sciences USA* **77**, 2023–2027.

Gabashvili, I. S., Agrawal, R. K., Spahn, C. M. T., Grassucci, R. A., Svergun, D. I., Frank, J. & Penczek, P. (2000). Solution structure of the *E. coli* 70S ribosome at 11·5 Ångstrom resolution. *Cell* **100**, 537–549.

Heide, H. G. (1982). Design and operation of cold stages. *Ultramicroscopy* **10**, 125–154.

Henderson, R. (1995). The potential and limitations of neutrons, electrons and X-rays for atomic-resolution microscopy of unstained biological molecules. *Quarterly Reviews of Biophysics* **28**, 171–193.

Henderson, R., Baldwin, J. M., Ceska, T. A., Zemlin, F., Beckmann, E. & Downing, K. H. (1990). Model for the structure of bacteriorhodopsin based on high-resolution electron cryo-microscopy. *Journal of Molecular Biology* **213**, 899–929.

Hirai, T., Heymann, J. A. W., Maloney, P. C. & Subramaniam, S. (2003). Structural model for 12-helix

transporters belonging to the major facilitator superfamily. *Journal of Bacteriology* **185**, 1712–1718.

HIRAI, T., HEYMANN, J. A. W., SHI, D., SARKER, R., MALONEY, P. C. & SUBRAMANIAM, S. (2002). Three-dimensional structure of a bacterial oxalate transporter. *Nature Structural Biology* **9**, 597–600.

HOROWITZ, R. A., AGARD, D. A., SEDAT, J. W. & WOODCOCK, C. L. (1994). The 3-dimensional architecture of chromatin *in-situ* – electron tomography reveals fibers composed of a continuously variable zigzag nucleosomal ribbon. *Journal of Cell Biology* **125**, 1–10.

HUISKONEN, J. T., KIVELA, H. M., BAMFORD, D. H. & BUTCHER, S. J. (In Press). The PM2 virion has a novel organization with an internal membrane and pentameric receptor binding spikes. *Nature Structural and Molecular Biology*.

JAP, B. K., WALIAN, P. J. & GEHRING, K. (1991). Structural architecture of an outer-membrane channel as determined by electron crystallography. *Nature* **350**, 167–170.

JENG, T. W., CROWTHER, R. A., STUBBS, G. & CHIU, W. (1989). Visualization of alpha-helices in tobacco mosaic virus by cryo-electron microscopy. *Journal of Molecular Biology* **205**, 251–257.

JIANG, W., LI, Z. L., ZHANG, Z. X., BAKER, M. L., PREVELIGE, P. E. & CHIU, W. (2003). Coat protein fold and maturation transition of bacteriophage P22 seen at subnanometer resolutions. *Nature Structural Biology* **10**, 131–135.

KIMURA, Y., VASSYLYEV, D. G., MIYAZAWA, A., KIDERA, A., MATSUSHIMA, M., MITSUOKA, K., MURATA, K., HIRAI, T. & FUJIYOSHI, Y. (1997). Surface of bacteriorhodopsin revealed by high-resolution electron crystallography. *Nature* **389**, 206–211.

KREBS, A., EDWARDS, P. C., VILLA, C., LI, J. & SCHERTLER, G. F. X. (2003). The three-dimensional structure of bovine rhodopsin determined by electron cryo-microscopy. *Journal of Biological Chemistry* **278**, 50217–50225.

KÜHLBRANDT, W., WANG, D. N. & FUJIYOSHI, Y. (1994). Atomic model of plant light-harvesting complex by electron crystallography. *Nature* **367**, 614–621.

KUNJI, E. R. S., VON GRONAU, S., OESTERHELT, D. & HENDERSON, R. (2000). The three-dimensional structure of halorhodopsin to 5 Ångstrom by electron crystallography: a new unbending procedure for two-dimensional crystals by using a global reference structure. *Proceedings of the National Academy of Sciences USA* **97**, 4637–4642.

LEIFER, D. & HENDERSON, R. (1983). Three-dimensional structure of orthorhombic purple membrane at 6·5 Å resolution. *Journal of Molecular Biology* **163**, 451–466.

LI, H. L., DEROSIER, D. J., NICHOLSON, W. V., NOGALES, E. & DOWNING, K. H. (2002). Microtubule structure at 8 Ångstrom resolution. *Structure* **10**, 1317–1328.

LUDTKE, S. J., JAKANA, J., SONG, J. L., CHUANG, D. T. & CHIU, W. (2001). A 11·5 angstrom single particle reconstruction of GroEL using EMAN. *Journal of Molecular Biology* **314**, 253–262.

MANCINI, E. J., CLARKE, M., GOWEN, B. E., RUTTEN, T. & FULLER, S. D. (2000). Cryo-electron microscopy reveals the functional organization of an enveloped virus, Semliki Forest virus. *Molecular Cell* **5**, 255–266.

MATADEEN, R., PATWARDHAN, A., GOWEN, B., ORLOVA, E. V., PAPE, T., MUELLER, F., BRIMACOMBE, R. & VAN HEEL, M. (1999). The *E. coli* 50S ribosomal subunit at 7·5 Å resolution. *Structure* **7**, 1575–1583.

MATSUI, Y., SAKAI, K., MURAKAMI, M., SHIRO, Y., ADACHI, S., OKUMURA, H. & KOUYAMA, T. (2002). Specific damage induced by X-ray radiation and structural changes in the primary photoreaction of bacteriorhodopsin. *Journal of Molecular Biology* **324**, 469–481.

MEDALIA, O., WEBER, I., FRANGAKIS, A. S., NICASTRO, D., GERISCH, G. & BAUMEISTER, W. (2002). Macromolecular architecture in eukaryotic cells visualized by cryo-electron tomography. *Science* **298**, 1209–1213.

MITRA, A. K., REN, G., REDDY, V. S., CHENG, A. & FROGER, A. (2002). The architecture of a water-selective pore in the lipid bilayer visualized by electron crystallography in vitreous ice. In: Novartis Foundation Symposium: *Ion Channels: From Atomic Resolution Physiology to Functional Genomics* **243**, 33–50.

MIYAZAWA, A., FUJIYOSHI, Y. & UNWIN, N. (2003). Structure and gating mechanism of the acetylcholine receptor pore. *Nature* **423**, 949–955.

MURATA, K., MITSUOKA, K., HIRAI, T., WALZ, T., AGRE, P., HEYMANN, J. B., ENGEL, A. & FUJIYOSHI, Y. (2000). Structural determinants of water permeation through aquaporin-1. *Nature* **407**, 599–605.

NAKAGAWA, A., MIYAZAKI, N., TAKA, J., NAITOW, H., OGAWA, A., FUJIMOTO, Z., MIZUNO, H., HIGASHI, T., WATANABE, Y., OMURA, T., CHENG, R. H. & TSUKIHARA, T. (2003). The atomic structure of Rice dwarf virus reveals the self-assembly mechanism of component proteins. *Structure* **11**, 1227–1238.

NOGALES, E., WOLF, S. G. & DOWNING, K. H. (1998). Structure of the alpha beta tubulin dimer by electron crystallography. *Nature* **391**, 199–203.

ORLOVA, E. V., GOWEN, B., DROGE, A., STIGE, A., WEISE, F., LURZ, R., VAN HEEL, M. & TAVARES, P. (2003). Structure of a viral DNA gatekeeper at 10 Å resolution by cryo-electron microscopy. *EMBO Journal* **22**, 1255–1262.

O'TOOLE, E. T., WINEY, M. & MCINTOSH, J. R. (1999). High-voltage electron tomography of spindle pole bodies and early mitotic spindles in the yeast Saccharomyces cerevisiae. *Molecular Biology of the Cell* **10**, 2017–2031.

RANSON, N. A., FARR, G. W., ROSEMAN, A. M., GOWEN, B., FENTON, W. A., HORWICH, A. L. & SAIBIL, H. R. (2001). ATP-bound states of GroEL captured by cryo-electron microscopy. *Cell* **107**, 869–879.

Rhee, K. H., Morriss, E. P., Barber, J. & Kuhlbrandt, W. (1998). Three-dimensional structure of the plant photosystem II reaction centre at 8 Ångstrom resolution. *Nature* **396**, 283–286.

Rosenthal, P. B., Crowther, R. A. & Henderson, R. (2003). Appendix: an objective criterion for resolution assessment in single-particle electron microscopy. *Journal of Molecular Biology* **333**, 743–745.

Rosenthal, P. B. & Henderson, R. (2003). Optimal determination of particle orientation, absolute hand, and contrast loss in single-particle electron cryomicroscopy. *Journal of Molecular Biology* **333**, 721–745.

Samatey, F. A., Imada, K., Nagashima, S., Vonderviszt, F., Kumasaka, T., Yamamoto, M. & Namba, K. (2001). Structure of the bacterial flagellar protofilament and implications for a switch for supercoiling. *Nature* **410**, 331–337.

Schmidt-Krey, I., Mitsuoka, K., Hirai, T., Murata, K., Cheng, Y., Fujiyoshi, Y., Morgenstern, R. & Hebert, H. (2000). The three-dimensional map of microsomal glutathione transferase 1 at 6 Ångstrom resolution. *EMBO Journal* **19**, 6311–6316.

Stahlberg, H., Braun, T., de Groot, B., Philippsen, A., Borgnia, M. J., Agre, P., Kühlbrandt, W. & Engel, A. (2000). The 6·9-Ångstrom structure of GlpF: a basis for homology modeling of the glycerol channel from *Escherichia coli*. *Journal of Structural Biology* **132**, 133–141.

Stewart, P. L., Burnett, R. M., Cyrklaff, M. & Fuller, S. D. (1991). Image reconstruction reveals the complex molecular organisation of adenovirus. *Cell* **67**, 145–154.

Stewart, P. L., Fuller, S. D. & Burnett, R. M. (1993). Difference imaging of adenovirus: bridging the resolution gap between X-ray crystallography and electron microscopy. *EMBO Journal* **12**, 2589–2599.

Taylor, K. A. & Glaeser, R. M. (1976). Electron microscopy of frozen, hydrated protein crystals. *Journal of Ultrastructural Research* **55**, 448–456.

Toyoshima, C., Nakasako, M., Nomura, H. & Ogawa, H. (2000). Crystal structure of the calcium pump of sarcoplasmic reticulum at 2·6 Ångstrom resolution. *Nature* **405**, 647–655.

Tsygannik, I. N. & Baldwin, J. M. (1987). Three-dimensional structure of deoxycholate-treated purple membrane at 6 Å resolution and molecular averaging of three crystal forms of bacteriorhodopsin. *European Biophysics Journal* **14**, 263–272.

Ubarretxena-Belandia, I., Baldwin, J. M., Schuldiner, S. & Tate, C. G. (2003). Three-dimensional structure of the bacterial multidrug transporter EmrE shows it is an asymmetric homodimer. *EMBO Journal* **22**, 6175–6181.

Unger, V. M., Hargrave, P. A., Baldwin, J. M. & Schertler, G. F. X. (1997). Arrangement of rhodopsin transmembrane alpha-helices. *Nature* **389**, 203–206.

Unger, V. M., Kumar, N. M., Gilula, N. B. & Yeager, M. (1999). Three-dimensional structure of arecombinant gap junction membrane channel. *Science* **283**, 1176–1180.

Valle, M., Zavialov, A., Li, W., Stagg, S. M., Sengupta, J., Nielsen, R. C., Nissen, P., Harvey, S. C., Ehrenberg, M. & Frank, J. (2003). Incorporation of aminoacyl-tRNA into the ribosome as seen by cryo-electron microscopy. *Nature Structural Biology* **10**, 899–906.

van Heel, M., Gowen, B., Matadeen, R., Orlova, E. V., Finn, R., Pape, T., Cohen, D., Stark, H., Schmidt, R., Schatz, M. & Patwardhan, A. (2000). Single-particle electron cryo-microscopy: towards atomic resolution. *Quarterly Reviews of Biophysics* **33**, 307–369.

Williams, K. A. (2000). Three-dimensional structure of the ion-coupled transport protein NhaA. *Nature* **403**, 112–115.

Wynne, S. A., Crowther, R. A. & Leslie, A. G. W. (1999). The crystal structure of the human hepatitis B virus capsid. *Molecular Cell* **3**, 771–780.

Yonekura, K., Maki-Yonekura, S. & Namba, K. (2003). Complete atomic model of the bacterial flagellar filament by electron cryo-microscopy. *Nature* **424**, 643–650.

Zhang, P. J., Toyoshima, C., Yonekura, K., Green, N. M. & Stokes, D. L. (1998). Structure of the calcium pump from sarcoplasmic reticulum at 8-Ångstrom resolution. *Nature* **392**, 835–839.

Zhang, W., Chipman, P. R., Corver, J., Johnson, P. R., Zhang, Y., Mukhopadhyay, S., Baker, T. S., Strauss, J. H., Rossmann, M. G. & Kuhn, R. J. (2003a). Visualization of membrane protein domains by cryo-electron microscopy of dengue virus. *Nature Structural Biology* **10**, 907–912.

Zhang, W., Mukhopadhyay, S., Pletnev, V., Baker, T. S., Kuhn, R. J. & Rossmann, M. G. (2002). Placement of the structural proteins in Sindbis virus. *Journal of Virology* **76**, 11645–11658.

Zhang, X., Walker, S. B., Chipman, P. R., Nibert, M. L. & Baker, T. S. (2003b). Reovirus polymerase λ3 localized by electron cryo-microscopy of virions at 7·6 Å resolution. *Nature Structural Biology* **10**, 1011–1018.

Zhou, Z. H., Baker, M. L., Jiang, W., Dougherty, M., Jakana, J., Dong, G., Lu, G. Y. & Chiu, W. (2001). Electron cryo-microscopy and bioinformatics suggest protein fold models for rice dwarf virus. *Nature Structural Biology* **8**, 868–873.

Zhou, Z. H., Dougherty, M., Jakana, J., He, J., Rixon, F. J. & Chiu, W. (2000). Seeing the herpesvirus capsid at 8·5 Ångstrom. *Science* **288**, 877–880.

Zhou, Z. H., Zhang, H., Jakana, J., Lu, X. Y. & Zhang, J. G. (2003). Cytoplasmic polyhedrosis virus structure at 8 angstrom by electron cryo-microscopy: structural basis of capsid stability and mRNA processing regulation. *Structure* **11**, 651–663.